

Assembling two Dy₂ single-molecule magnets with different energy barriers via fine-tuning the geometries of Dy^{III} sites

Dawei Li,^a Man-Man Ding,^b Yu Ge,^a David Felipe Tello Yepes,^d Mingyuan Sun,^a Muhammad Saleem Najib,^d Yahong Li,^{*a} Yi-Quan Zhang^{*b} and Jin-lei Yao^{*c}

^a College of Chemistry, Chemical Engineering and Materials Science Soochow University, Suzhou 215123, China

E-mail: liyahong@suda.edu.cn.

^b Jiangsu Key Laboratory for NSLSCS, School of Physical Science and Technology, Nanjing Normal University, Nanjing 210023, China

E-mail: zhangyiquan@njnu.edu.cn

^c Jiangsu Key Laboratory of Micro and Nano Heat Fluid Flow Technology and Energy Application, School of Mathematics and Physics, Suzhou University of Science and Technology, Suzhou 215009, China

E-mail: jlyao@usts.edu.cn.

^d College of Environmental Engineering, University of Waterloo, Waterloo N2L3G1, Canada

Supplementary Information Contents

1. ¹ H, ¹³ C NMR spectra of H ₂ L ¹ and H ₂ L ²	2
2. PXRD patterns of 1 and 2	4
3. IR spectra of H ₂ L ¹ , H ₂ L ² , 1 and 2	5
4. Selected bond lengths and angles for 1 and 2	6
5. SHAPE program details for 1 and 2	9
6. Examples of eight-coordinated Dy ₂ SMMs bearing [Dy ₂ O ₂] moieties	10
7. Int versus T ⁻¹ plots for complexes 1 and 2 at high temperature	11
8. Temperature dependence of the χ'' plots for complex 1 and the diluted sample at indicated frequencies under 0 Oe (Fig. S6), 200 Oe (Fig. S7) and 4000 Oe (Fig. S8).....	12
9. Plot of ln(τ) vs 1/T for 1 and the diluted sample.....	15
10. Best fitted parameters for complexes 1 and 2 under 0 Oe dc field	16
11. Computational details.....	18

1. ^1H , ^{13}C NMR spectra of H_2L^1 and H_2L^2

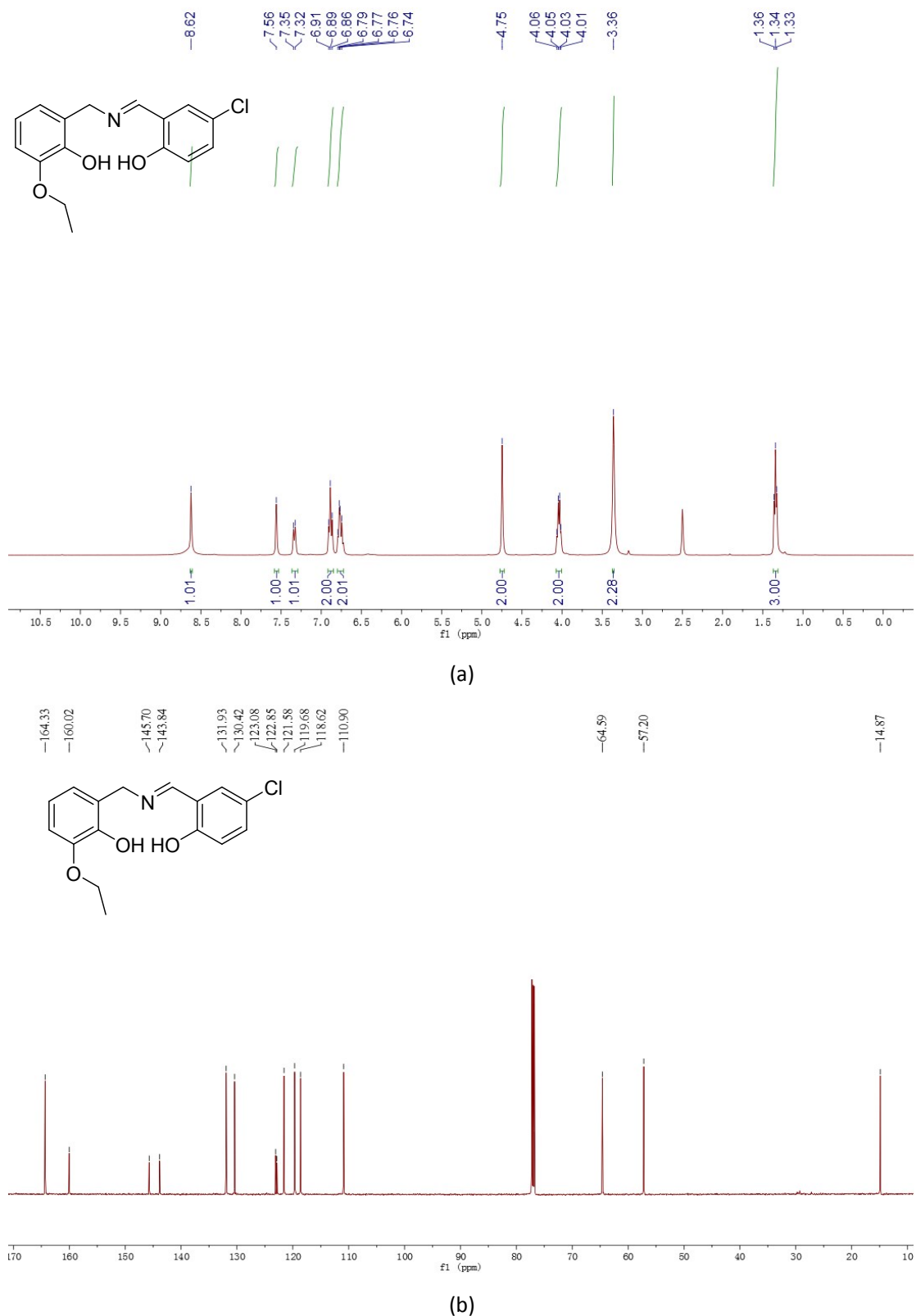
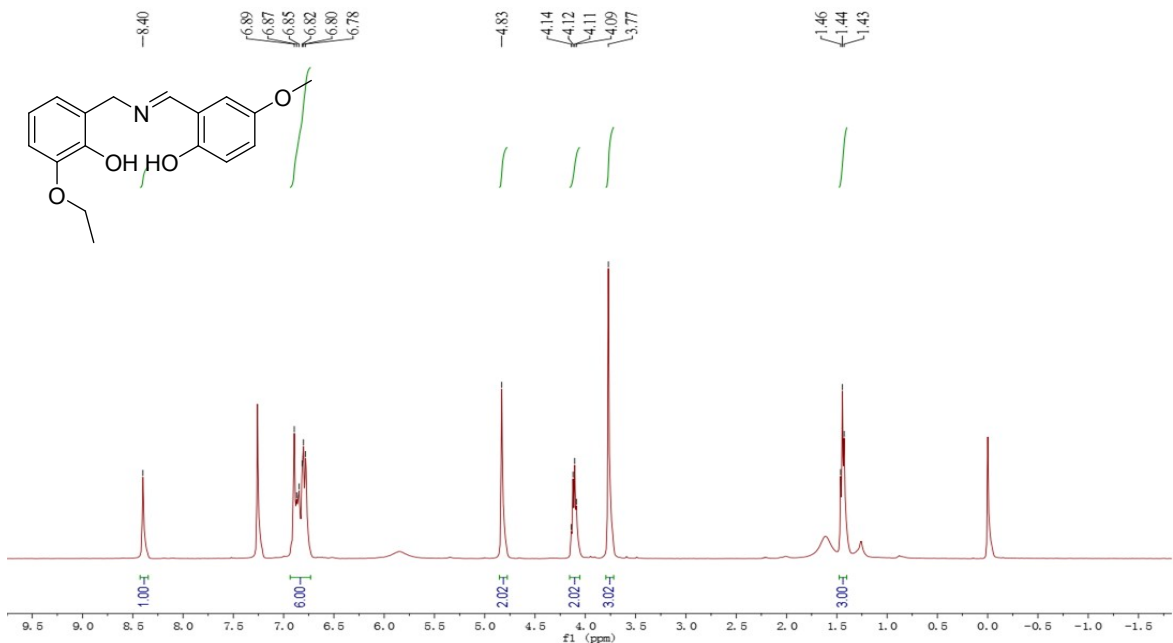


Fig. S1 The ^1H NMR (a) and ^{13}C NMR (b) spectra of H_2L^1 .



(c)

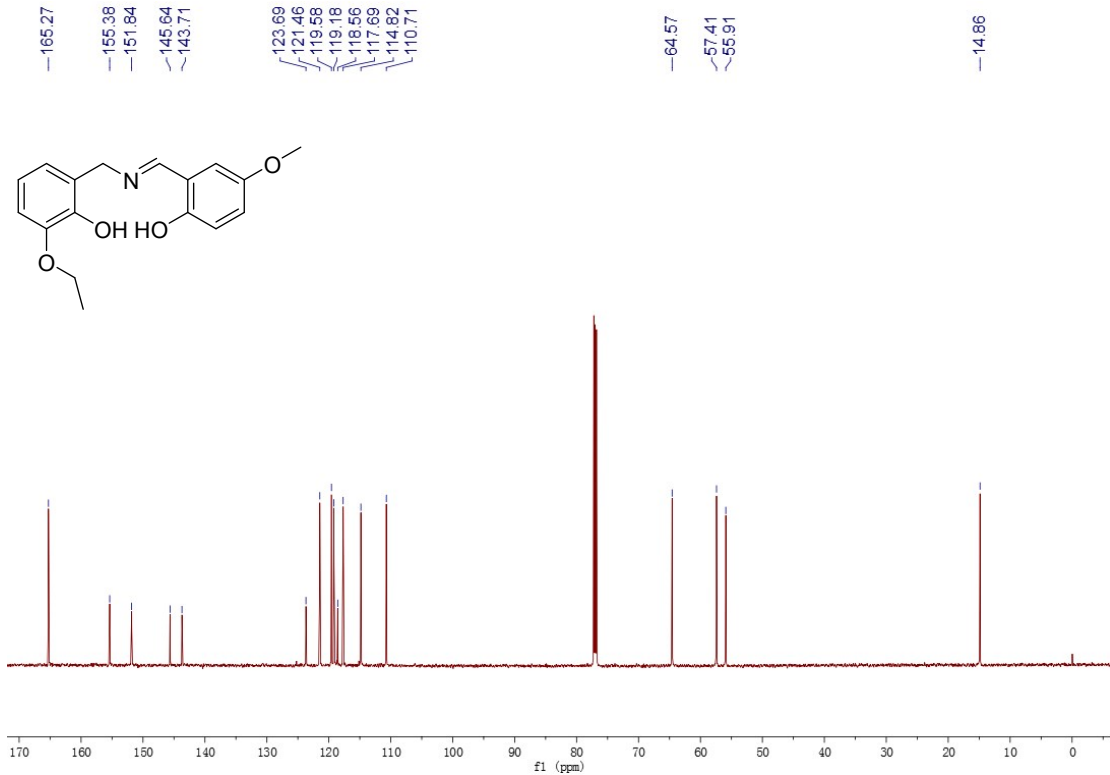
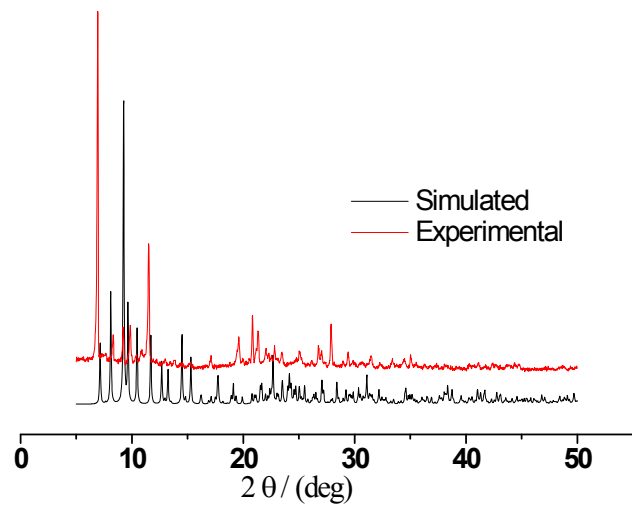
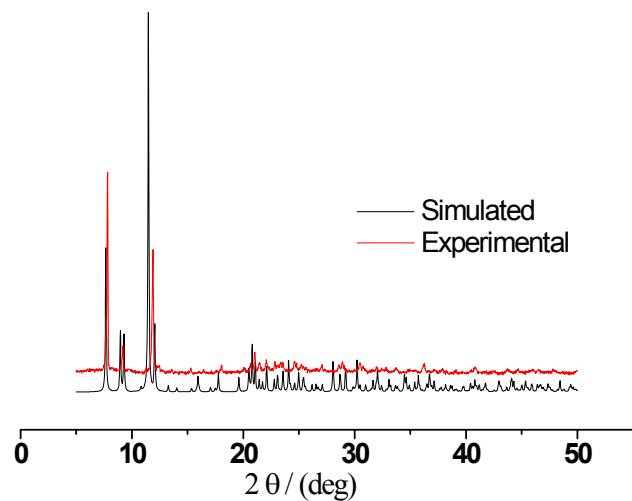


Fig. S2 The ^1H NMR (c) and ^{13}C NMR (d) spectra of H_2L^2 .

2. PXRD patterns of **1** and **2**



(a)



(b)

Fig. S3 PXRD patterns of **1**(a) and **2** (b).

3. IR spectra of H_2L^1 , H_2L^2 , **1** and **2**

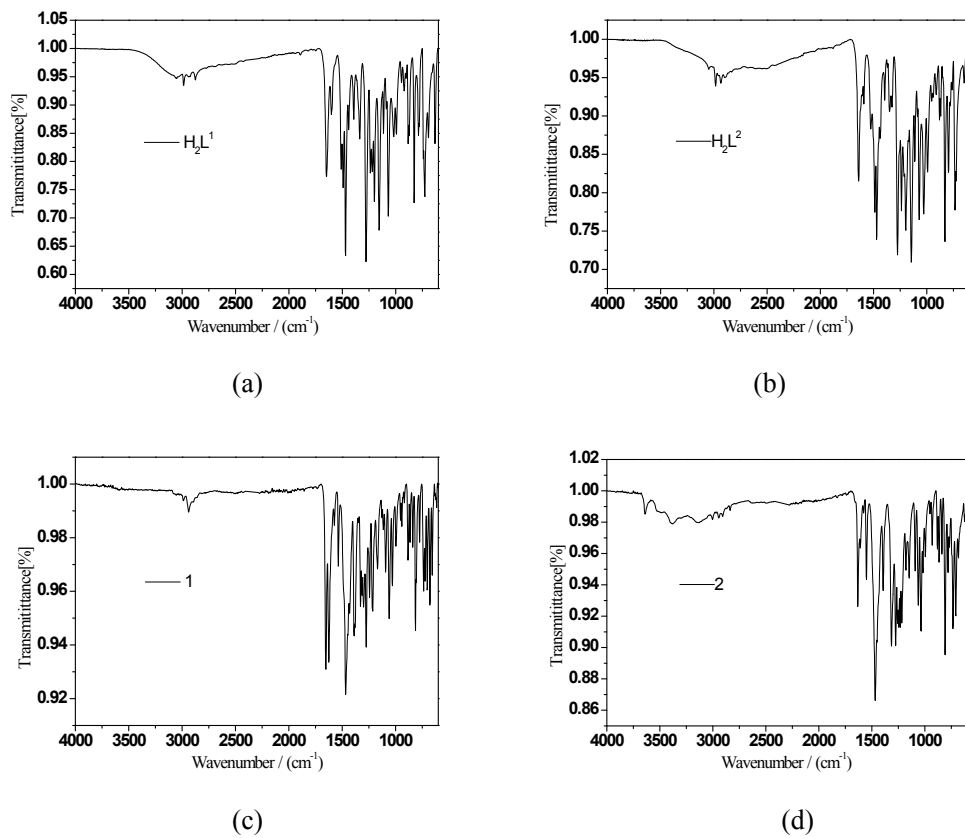


Fig. S4 FT-IR spectra of H_2L^1 (a), H_2L^2 (b), **1** (c) and **2** (d).

4. Selected bond lengths and angles for **1** and **2**

Table S1 Selected bond lengths (\AA) and angle ($^\circ$) for complexes **1** and **2**

1			
Dy1-O7	2.480(8)	Dy2-O9	2.315(9)
Dy1-O10	2.175(8)	Dy2-O1	2.391(7)
Dy1-O9	2.282(7)	Dy2-O15	2.478(11)
Dy1-O1	2.370(9)	Dy2-O2	2.216(8)
Dy1-O3	2.370(8)	Dy2-O13	2.498(10)
Dy1-N3	2.531(11)	Dy2-O12	2.446(9)
Dy1-O4	2.479(11)	Dy2-O11	2.298(9)
Dy1-O5	2.454(10)	Dy2-N1	2.452(11)
O7-Dy1-N3	149.0(3)	O9-Dy2-O1	67.6(3)
O10-Dy1-O7	78.6(3)	O9-Dy2-O15	66.1(3)
O10-Dy1-O9	149.0(3)	O9-Dy2-O13	73.9(3)
O10-Dy1-O1	141.4(3)	O9-Dy2-O12	84.1(3)
O10-Dy1-O3	83.7(3)	O9-Dy2-N1	142.6(3)
O10-Dy1-N3	74.5(3)	O1-Dy2-O15	120.1(3)
O10-Dy1-O4	86.1(4)	O1-Dy2-O13	123.5(3)
O10-Dy1-O5	91.2(4)	O1-Dy2-O12	83.7(3)
O9-Dy1-O7	132.3(3)	O1-Dy2-N1	78.1(3)
O9-Dy1-O1	68.5(3)	O15-Dy2-O13	75.8(3)
O9-Dy1-O3	99.4(3)	O2-Dy2-O9	140.5(3)
O9-Dy1-N3	76.1(3)	O2-Dy2-O1	151.9(3)
O9-Dy1-O4	77.9(3)	O2-Dy2-O15	81.1(3)
O9-Dy1-O5	98.9(3)	O2-Dy2-O13	77.2(3)
O1-Dy1-O7	65.5(3)	O2-Dy2-O12	98.8(3)
O1-Dy1-N3	133.4(3)	O2-Dy2-O11	85.7(4)
O1-Dy1-O4	122.0(3)	O2-Dy2-N1	75.2(3)

O1-Dy1-O5	88.5(4)	O12-Dy2-O15	125.7(3)
O3-Dy1-O7	84.1(3)	O12-Dy2-O13	52.0(3)
O3-Dy1-O1	79.0(3)	O12-Dy2-N1	77.7(3)
O3-Dy1-N3	77.9(3)	O11-Dy2-O9	106.3(3)
O3-Dy1-O4	154.4(3)	O11-Dy2-O1	82.3(3)
O3-Dy1-O5	152.2(4)	O11-Dy2-O15	76.5(3)
O4-Dy1-O7	116.8(3)	O11-Dy2-O13	149.3(3)
O4-Dy1-N3	76.7(3)	O11-Dy2-O12	157.7(4)
O5-Dy1-O7	68.1(4)	O11-Dy2-N1	82.5(4)
O5-Dy1-N3	127.1(4)	N1-Dy2-O15	149.3(3)
O5-Dy1-O4	51.2(4)	N1-Dy2-O13	116.5(3)
Dy1-O9-Dy2	113.0(3)	Dy1-O1-Dy2	107.2(3)

2

Dy1-O4	2.427(7)	Dy1-O2	2.170(6)
Dy1-O1	2.301(6)	Dy1-O3	2.372(6)
Dy1-O11	2.356(5)	Dy1-O5	2.484(6)
Dy1-O81	2.507(6)	Dy1-N1	2.460(6)
O1-Dy11	2.356(5)	O8-Dy11	2.507(6)
O4-Dy1-O81	72.9(2)	O3-Dy1-O5	153.4(2)
O4-Dy1-O5	51.9(2)	O3-Dy1-N1	78.8(2)
O4-Dy1-N1	124.7(2)	O5-Dy1-O81	123.1(2)
O1-Dy1-O4	99.2(2)	N1-Dy1-O81	146.0(2)
O11-Dy1-O4	91.5(2)	N1-Dy1-O5	74.6(2)
O1-Dy1-O11	67.0(2)	N2-O4-Dy1	97.5(5)
O1-Dy1-O81	131.37(19)	Dy1-O1-Dy11	106.0(2)
O11-Dy1-O81	65.39(19)	O2-Dy1-O1	150.1(2)
O1-Dy1-O3	99.9(2)	O2-Dy1-O11	142.6(2)
O11-Dy1-O3	78.0(2)	O2-Dy1-O81	78.4(2)

O1-Dy1-O5	76.2(2)	O2-Dy1-O3	86.9(2)
O11-Dy1-O5	122.4(2)	O2-Dy1-O5	84.7(2)
O11-Dy1-N1	133.7(2)	O2-Dy1-N1	74.6(2)
O1-Dy1-N1	78.3(2)	O3-Dy1-O4	152.4(2)
O2-Dy1-O4	86.3(2)	O3-Dy1-O81	79.5(2)

Symmetry transformations used to generate equivalent atoms: $^{11}\text{-X}$, $+\text{Y}$, $3/2\text{-Z}$

5. SHAPE program details for **1** and **2**

Table S2 Agreement factors between the coordination polyhedron of the Dy^{III} ions in Dy₂ and the various ideal polyhedrons calculated by the SHAPE program.

Agreement factors for Dy ^{III} ion in complexes	<i>TDD-8(D_{2d})</i>	<i>SAPR-8(D_{4d})</i>
Dy ^{III} in 1	2.737	4.739
	2.038	1.911
Dy ^{III} in 2	2.584	4.860
	2.584	4.860

TDD-8(D_{2d}) = Triangular dodecahedron

SAPR-8(D_{4d}) = Square antiprism

6. Examples of eight-coordinated Dy₂ SMMs bearing [Dy₂O₂] moieties

Table S3 Examples of eight-coordinated Dy₂ SMMs bearing [Dy₂O₂] moieties

Complexes	Solvent ligand	Dono rs	Sy mm etry	Magnetic behavior	Dy···Dy distance / Å	Dy-O-Dy angle /°	τ_0/s	$U_{\text{eff}}/K_B(\text{K})$
[Dy ₂ (bfopen) ₂ (H ₂ O) ₂]·2I ⁻ ^{S1a}	H ₂ O	N ₄ O ₄	D_{4d}	AF	3.845	109.45	3.68×10^{-6}	20.9 (0 Oe) 26.9 (1200 Oe)
[Dy ₂ (bcbpen) ₂ (H ₂ O) ₂]·2I ⁻ ·0.5H ₂ O ^{S1a}	H ₂ O	N ₄ O ₄	D_{4d}	AF	3.861	110.01	6.79×10^{-7}	72.7 (0 Oe)
[Dy ₂ (hmi) ₂ (NO ₃) ₂ (MeOH) ₂] ^{S1b}	MeOH	NO ₇	/	F	3.750	106.41	3×10^{-7}	56 (0 Oe)
[Dy ₂ (L ¹) ₂ (NO ₃) ₂ (MeOH) ₂] ^{S1c}	MeOH	NO ₇	D_{2d}	F	3.787	109.32	2.66×10^{-7}	198.8 (0 Oe)
[Dy ₂ (L ¹) ₂ (NO ₃) ₂ (EtOH) ₂] ^{S1c}	EtOH	NO ₇	D_{2d}	F	3.774	108.84	2.16×10^{-6}	131.3 (0 Oe)
[Dy ₂ (L ²) ₂ (NO ₃) ₂ (MeOH) ₂] ·2MeOH ^{S1d}	MeOH	NO ₇	D_{2d}	F	3.7353	107.73	3.21×10^{-5}	51.97 (0 Oe)
Dy ₂ (L ³) ₂ (NO ₃) ₂ (MeOH) ₂ ^{S1d}	MeOH	NO ₇	D_{4d}	F	3.8397	111.13 111.69	6.74×10^{-6}	87.16 (0 Oe)
[Dy ₂ (L ⁴) ₂ (DBM) ₂ (DMA) ₂] ·2DMA ^{S1e}	DMA	NO ₇	C_{2v}	AF	3.7198	105.3	2.74×10^{-8}	77 (0 Oe)
[Dy ₂ (L ⁴) ₂ (DBM) ₂ (DMF) ₂] ^{S1e}	DMF	NO ₇	C_{2v}	AF	3.7270	106	1.36×10^{-6}	24 (0 Oe)
[Dy ₂ (L ⁵) ₂ (piv) ₂] ^{S1f}	/	N ₃ O ₅	D_{2h}	AF	3.798	110.19	3.06×10^{-6}	40.32 (0 Oe)
[Dy ₂ (L ⁶) ₂ (piv) ₂] ^{S1f}	/	N ₃ O ₅	D_{2h}	AF	3.810	106.74	9.19×10^{-6}	31.67 (0 Oe)
[Dy ₂ (L ⁷) ₂ (piv) ₂]·2MeCN ^{S1f}	/	N ₃ O ₅	D_{2h}	AF	3.8350/3. 8226	109.07/10 8.38	2.17×10^{-6}	33.53 (0 Oe)
[Dy ₂ (L ⁸) ₂ (NO ₃) ₂ (EtOH)(DM F)]·2EtOH ^[this work]	EtOH	NO ₇	D_{2d}	F	3.8326	113.0/107 .2	4.64×10^{-6}	86.91 (0 Oe)
[Dy ₂ (L ⁹) ₂ (NO ₃) ₂ (MeOH) ₂] ^[this work]	MeOH	NO ₇	D_{2d}	F	3.7193	106.0	3.88×10^{-6}	93.70 (0 Oe)
<p>H₂bfopen = N,N'-bis-(2-hydroxy-5-fluoro-benzyl)-N,N'-bis-(pyridin-2-ylmethyl)ethylenediamine, H₂bcbpen = N,N'-bis-(2-hydroxy-5-chloro-benzyl)-N,N'-bis-(pyridin-2-ylmethyl)ethylenediamine, H₂hmi = (2-hydroxy-3-methoxyphenyl)methylene (isonicotino)hydrazine, H₂L¹ = 2-ethoxy-6-(((2-hydroxy-3-methoxy benzyl)imino)methyl)phenol, H₂L² = 4-chloro-2-(((2-hydroxy-3-methoxybenzyl)imino)methyl)phenol, H₂L³ = 2-(((2-hydroxybenzylidene)amino)methyl)-6-methoxyphenol, H₂L⁴ = 2-hydroxy-N'-(2-hydroxy-3-methoxybenzylidene) benzohydrazide, HDBM = dibenzoylmethane, H₂L⁵ = N1,N3-bis (salicylaldehyde) diethylenetriamine, H₂L⁶ = N1,N3-bis(3-methoxysalicylidene)diethylenetriamine, H₂L⁷ = N1,N3-bis (5-chlorosalicylaldehyde)diethylenetriamine, H₂L⁸ = 4-chloro-2-((3-ethoxy-2-hydroxybenzyl)imino)methyl)phenol (this work), H₂L⁹ = 2-(((3-ethoxy-2-hydroxybenzyl)imino)methyl)-4-methoxyphenol (this work), F = ferromagnetic, AF = antiferromagnetic.</p>								

7. $\ln\tau$ versus T^{-1} plots for complexes **1** and **2** at high temperature

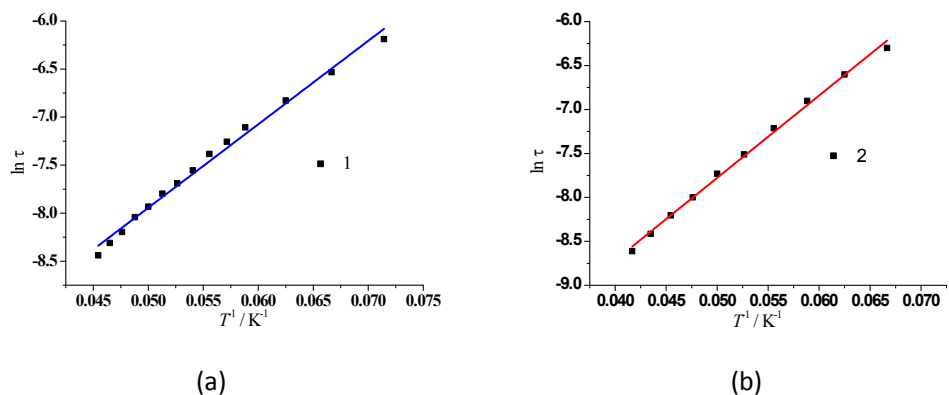
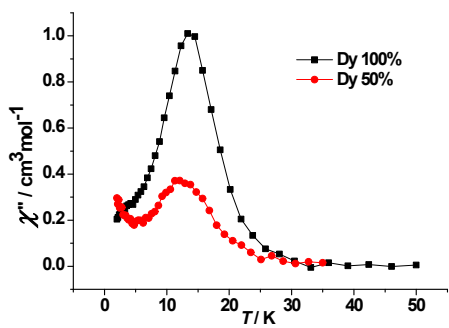


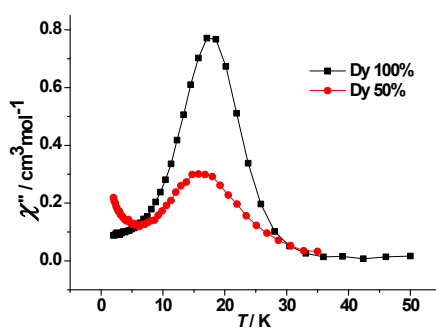
Fig. S5 $\ln\tau$ versus T^{-1} plots for **1** (a) and **2** (b) at the high temperature; the solid lines represent the least-squares fits of the experimental data to the Arrhenius law.

8. Temperature dependence of the χ'' plots for complex **1** and the diluted sample at indicated frequencies under 0 Oe (Fig. S6), 200 Oe (Fig. S7) , and 4000 Oe (Fig. S8).

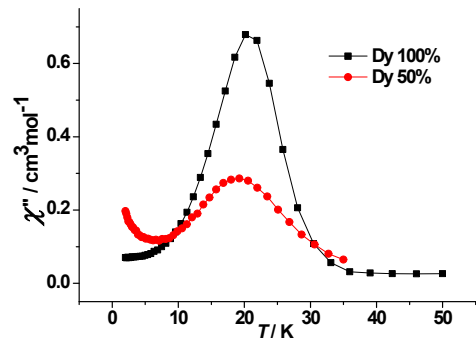
100 Hz Zero field



320 Hz Zero field



666 Hz Zero field



1000 Hz Zero field

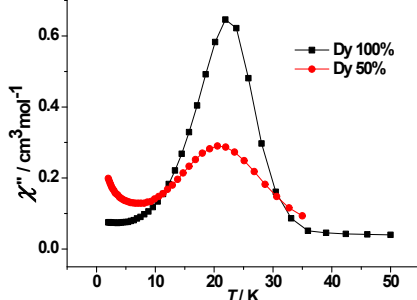
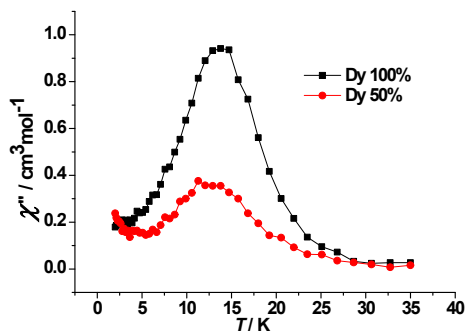
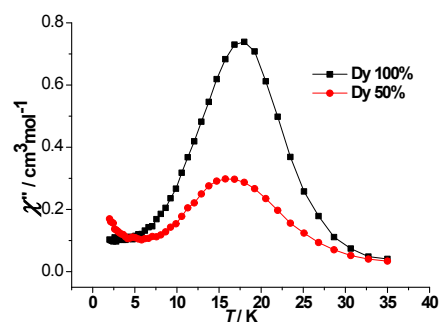


Fig. S6 Temperature dependence of the χ'' plots for complex **1** and the diluted sample at indicated frequencies and 0 Oe applied field.

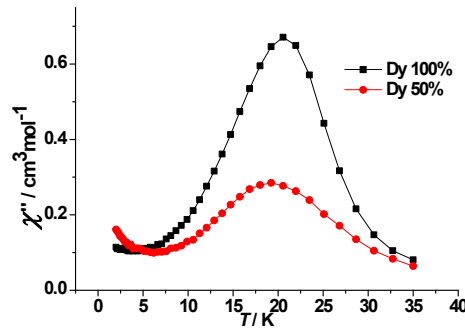
100 Hz 200 Oe field



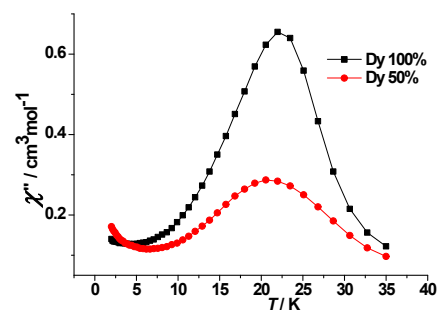
320 Hz 200 Oe field



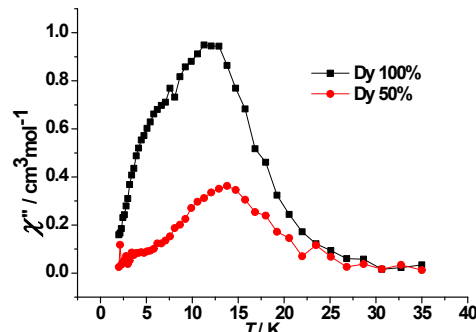
666 Hz 200 Oe field



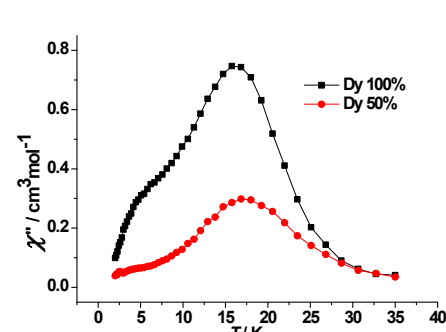
1000 Hz 200 Oe field

**Fig. S7** Temperature dependence of the χ'' plots for complex **1** and the diluted sample at indicated frequencies and 200 Oe applied field.

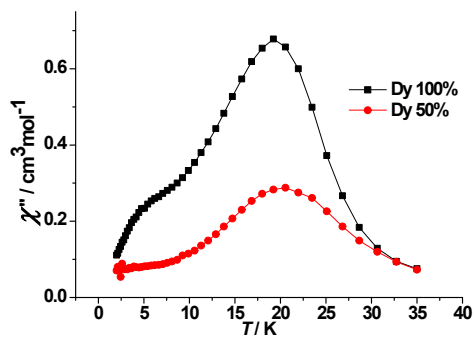
100 Hz 4000 Oe field



320 Hz 4000 Oe field



666 Hz 4000 Oe field



1000 Hz 4000 Oe field

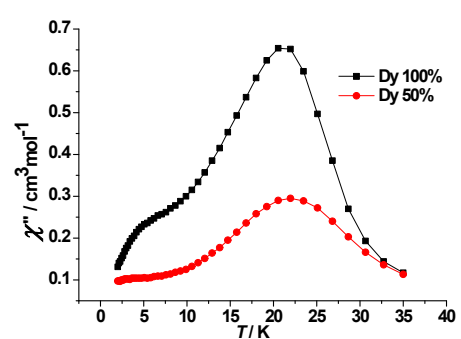


Fig. S8 Temperature dependence of the χ'' plots for complex **1** and the diluted sample at indicated frequencies and 4000 Oe applied field.

9. Plot of $\ln(\tau)$ vs $1/T$ for **1** and the diluted sample

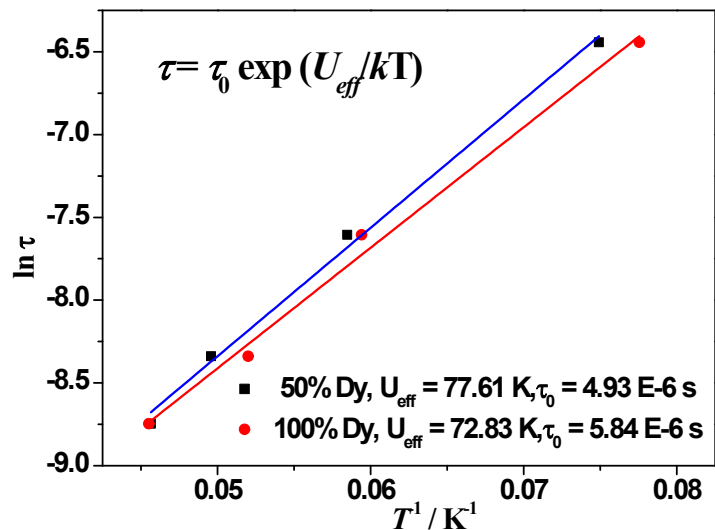


Fig. S9 Plot of $\ln(\tau)$ vs $1/T$ for two samples. The effective energy barriers (U_{eff}/K_B) obtained from the fits are indicated.

10. Best fitted parameters for complexes **1** and **2** under 0 Oe dc field

Table S4 Parameters from the fitting of the Cole-Cole plots of **1** according to the generalized Debye model.

Temperature / K	$\chi_s / \text{cm}^3\text{mol}^{-1}$	$\chi_T / \text{cm}^3\text{mol}^{-1}$	τ / s	α	R
10	2.30E-07	3.85E+00	1.04E-02	1.50E-01	6.59E-02
11	5.61E-07	3.19E+00	6.17E-03	1.20E-01	8.22E-02
12	9.61E-07	2.71E+00	3.88E-03	9.04E-02	1.82E-01
13	1.23E-06	2.53E+00	2.85E-03	1.01E-01	9.08E-02
14	1.88E-06	2.32E+00	2.05E-03	1.03E-01	3.36E-01
15	3.75E-06	2.13E+00	1.45E-03	8.17E-02	1.45E-01
16	6.54E-06	2.00E+00	1.08E-03	8.43E-02	1.33E-01
17	1.10E-05	1.85E+00	8.19E-04	8.57E-02	3.69E-01
17.5	1.71E-05	1.79E+00	7.06E-04	7.12E-02	9.17E-02
18	1.24E-05	1.75E+00	6.22E-04	7.48E-02	6.96E-02
18.5	1.82E-05	1.64E+00	5.23E-04	5.01E-02	2.94E-01
19	2.96E-05	1.59E+00	4.58E-04	4.29E-02	3.05E-01
19.5	3.88E-05	1.58E+00	4.11E-04	5.54E-02	1.37E-01
20	4.26E-05	1.53E+00	3.59E-04	4.62E-02	1.26E-01
20.5	1.58E-15	1.51E+00	3.22E-04	5.98E-02	5.70E-02
21	2.62E-15	1.42E+00	2.76E-04	2.56E-02	2.70E-01
21.5	3.31E-15	1.40E+00	2.46E-04	3.09E-02	2.16E-01
22	3.45E-15	1.37E+00	2.16E-04	2.24E-02	2.80E-01

Table S5 Parameters from the fitting of the Cole-Cole plots of **2** according to the generalized Debye model.

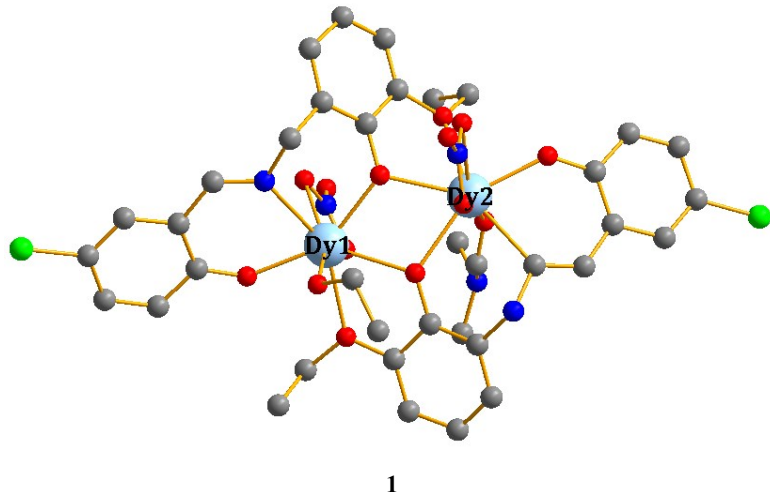
Temperature / K	$\chi_s / \text{cm}^3\text{mol}^{-1}$	$\chi_T / \text{cm}^3\text{mol}^{-1}$	τ / s	α	R
11	2.30E-02	3.15E+00	1.06E-02	7.46E-02	1.50E-01
12	5.66E-03	2.70E+00	6.26E-03	7.96E-02	5.15E-02

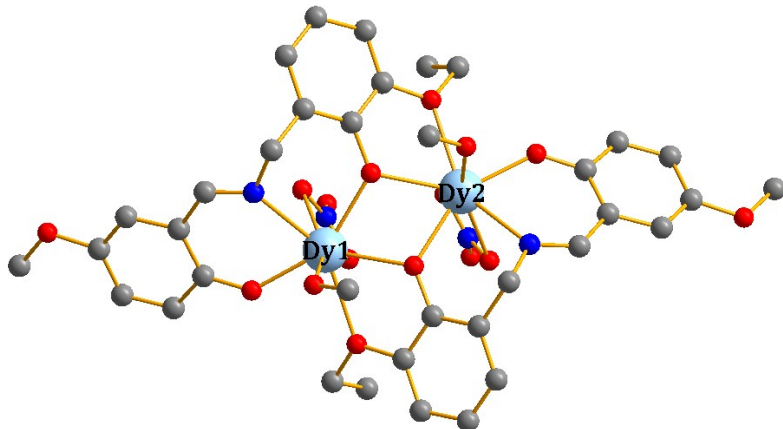
13	1.36E-15	2.33E+00	3.83E-03	6.90E-02	2.06E-01
14	8.25E-16	2.18E+00	2.63E-03	7.43E-02	1.58E-01
15	6.32E-16	2.01E+00	1.84E-03	7.04E-02	6.72E-02
16	6.61E-16	1.91E+00	1.36E-03	8.37E-02	1.22E-01
17	8.51E-16	1.80E+00	1.01E-03	8.35E-02	1.52E-01
18	6.56E-16	1.65E+00	7.37E-04	6.88E-02	1.08E-01
19	3.95E-16	1.51E+00	5.46E-04	4.44E-02	5.40E-01
20	4.83E-16	1.47E+00	4.39E-04	5.97E-02	2.56E-01
21	5.19E-17	1.35E+00	3.36E-04	2.10E-02	1.68E-01
22	8.81E-17	1.31E+00	2.73E-04	3.56E-02	4.31E-02
23	9.59E-17	1.25E+00	2.21E-04	3.23E-02	2.42E-01
24	1.02E-16	1.21E+00	1.82E-04	4.29E-02	1.70E-01

11. Computational details

Both of binuclear complexes **1** and **2** have two types of magnetic center Dy^{III} ions indicated as **1(Dy1)**, **1(Dy2)**, **2(Dy1)** and **2(Dy2)**, respectively. Complete-active-space self-consistent field (CASSCF) calculations on individual Dy^{III} fragments for **1** and **2** (see Figure S1 for the calculated complete structures of **1** and **2**) on the basis of single-crystal X-ray determined geometry have been carried out with MOLCAS 8.4^{S1} program package. Each individual Dy^{III} fragment in **1** and **2** was calculated keeping the experimentally determined structure of the corresponding compound while replacing the neighboring Dy^{III} ion by diamagnetic Lu^{III}.

The basis sets for all atoms are atomic natural orbitals from the MOLCAS ANO-RCC library: ANO-RCC-VTZP for Dy^{III}; VTZ for close N and O; VDZ for distant atoms. The calculations employed the second order Douglas-Kroll-Hess Hamiltonian, where scalar relativistic contractions were taken into account in the basis set and the spin-orbit couplings were handled separately in the restricted active space state interaction (RASSI-SO) procedure. Active electrons in 7 active spaces include all *f* electrons (CAS(9 in 7) in the CASSCF calculation. To exclude all the doubts, we calculated all the roots in the active space. We have mixed the maximum number of spin-free state which was possible with our hardware (all from 21 sextets, 128 from 224 quadruplets, 130 from 490 doublets for Dy^{II}. SINGLE_ANISO^{S2} program was used to obtain the energy levels, *g* tensors, magnetic axes, *et al.*, based on the above CASSCF/RASSI-SO calculations.





2

Fig. S10 Calculated complete structures of complexes **1** and **2**; H atoms are omitted.

Table S6 Calculated energy levels (cm^{-1}), \mathbf{g} (g_x , g_y , g_z) tensors and predominant m_J values of the lowest eight Kramers doublets (KDs) of individual Dy^{III} fragments for complexes **1** and **2** using CASSCF/RASSI-SO with MOLCAS 8.4.

KDs	1(Dy1)			1(Dy2)		
	E/cm^{-1}	\mathbf{g}	m_J	E/cm^{-1}	\mathbf{g}	m_J
1	0.0	0.002			0.002	
		0.003	$\pm 15/2$	0.0	0.004	$\pm 15/2$
		19.716			19.436	
2	240.5	0.094			0.055	
		0.113	$\pm 13/2$	167.2	0.064	$\pm 13/2$
		16.614			16.596	
3	375.6	0.771			0.269	
		0.851	$\pm 11/2$	327.7	0.352	$\pm 11/2$
		13.378			14.154	
4	453.7	4.182			3.515	
		6.072	$\pm 7/2$	425.8	4.336	$\pm 9/2$
		10.511			10.614	
5	501.6	7.990			11.443	
		6.413	$\pm 3/2$	479.9	6.615	$\pm 5/2$
		2.537			1.700	
6	541.0	2.627			0.459	
		6.114	$\pm 5/2$	548.4	2.882	$\pm 3/2$
		11.155			12.975	
7	593.1	0.267			1.116	
		1.130	$\pm 1/2$	592.0	3.540	$\pm 1/2$
		17.742			13.432	
8	657.8	0.083			0.262	
		0.220	$\pm 9/2$	644.4	0.670	$\pm 7/2$
		19.256			17.985	

KDs	2(Dy1)			2(Dy2)		
	E/cm^{-1}	\mathbf{g}	m_J	E/cm^{-1}	\mathbf{g}	m_J
1	0.0	0.002			0.002	
		0.003	$\pm 15/2$	0.0	0.003	$\pm 15/2$
		19.753			19.683	
2	243.1	0.077			0.075	
		0.095	$\pm 13/2$	243.6	0.093	$\pm 13/2$
		16.761			16.752	
3	387.0	0.629			0.621	
		0.688	$\pm 11/2$	387.8	0.681	$\pm 11/2$
		13.729			13.741	
4	483.0	2.971			2.998	
		3.286	$\pm 9/2$	484.2	3.309	$\pm 9/2$
		10.273			10.268	
5	538.6	3.112			3.088	
		5.556	$\pm 5/2$	540.3	5.541	$\pm 5/2$
		11.313			11.278	
6	594.5	0.557			0.568	
		2.414	$\pm 1/2$	596.0	2.448	$\pm 1/2$
		13.287			13.220	
7	622.9	0.257			0.258	
		0.577	$\pm 3/2$	624.2	0.568	$\pm 3/2$
		14.922			14.859	
8	673.6	0.225			0.227	
		0.502	$\pm 7/2$	674.9	0.517	$\pm 7/2$
		18.043			18.019	

Table S7 Wave functions with definite projection of the total moment $|m_J\rangle$ for the lowest two KDs of individual Dy^{III} fragments for complexes **1** and **2**.

	E/cm^{-1}	wave functions
1(Dy1)	0.0	97.6% $ \pm 15/2\rangle$
	240.5	85.2% $ \pm 13/2\rangle$ +10.0% $ \pm 9/2\rangle$
1(Dy2)	0.0	91.9% $ \pm 15/2\rangle$
	167.2	86.6% $ \pm 13/2\rangle$ +10.5% $ \pm 9/2\rangle$
2(Dy1)	0.0	97.6% $ \pm 15/2\rangle$
	243.1	82.3% $ \pm 13/2\rangle$ +10.2% $ \pm 9/2\rangle$ +4.4% $ \pm 11/2\rangle$
2(Dy2)	0.0	97.6% $ \pm 15/2\rangle$
	243.6	82.8% $ \pm 13/2\rangle$ +10.0% $ \pm 9/2\rangle$ +4.3% $ \pm 11/2\rangle$

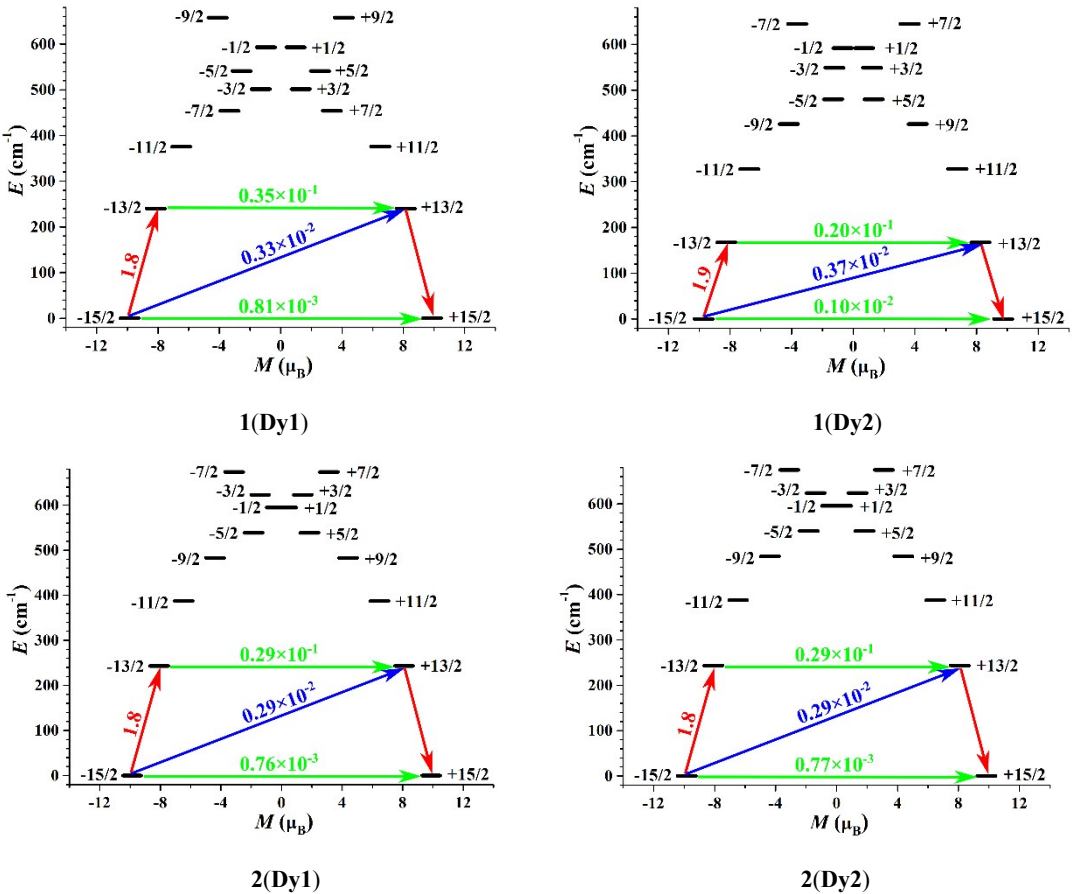


Fig. S11 Magnetization blocking barriers for individual Dy^{III} fragments in **1** and **2**. The thick black lines represent the KDs as a function of their magnetic moment along the magnetic axis. The green lines correspond to diagonal quantum tunneling of magnetization (QTM); the blue line represent off-diagonal relaxation process. The numbers at each arrow stand for the mean absolute value of the corresponding matrix element of transition magnetic moment.

To fit the exchange interactions in complexes **1** and **2**, we took two steps to obtain them. Firstly, we calculated individual Dy^{III} fragments using CASSCF/RASSI-SO to obtain the corresponding magnetic properties. Then, the exchange interactions between the magnetic centers were considered within the Lines model,^{S3} while the account of the dipole-dipole magnetic couplings were treated exactly. The Lines model is effective and has been successfully used widely in the research field of *d* and *f*-elements single-molecule magnets.^{S4}

For complexes **1** and **2**, there is only one type of %.

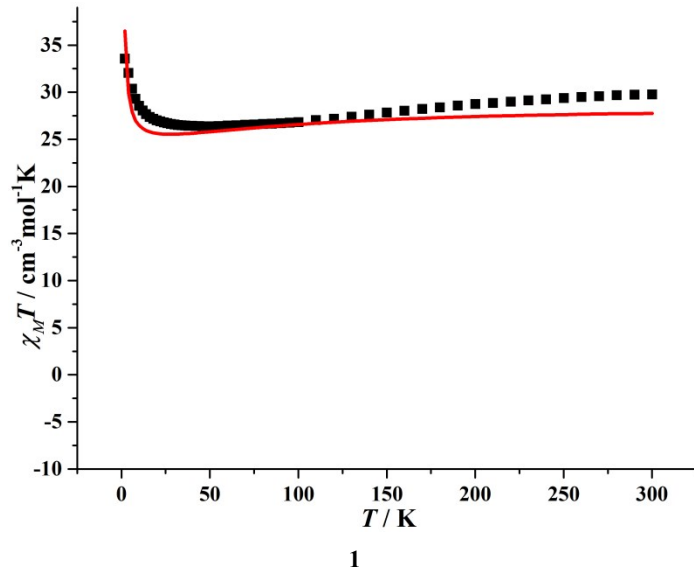
The Ising exchange Hamiltonian is:

$$\hat{H}_{\text{exch}} = -J \hat{S}_{\text{Dy1}} \hat{S}_{\text{Dy2}} \quad (1)$$

The \mathcal{J}_{total} is the parameter of the total magnetic interaction ($\mathcal{J}_{total} = \mathcal{J}_{dip} + \mathcal{J}_{exch}$) between magnetic center ions. The $S_{\text{Dy}} = 1/2$ is the ground pseudospin on the Dy^{III} site. The dipolar magnetic coupling can be calculated exactly, while the exchange coupling constant was fitted through comparison of the computed and measured magnetic susceptibilities using the POLY_ANISO program.^{S2}

Table S8 Exchange energies E (cm⁻¹), the energy difference between each exchange doublets Δ_t (cm⁻¹) and the main values of the g_z for the lowest two exchange doublets of **1** and **2**.

	1			2		
	E	Δ_t	g_z	E	Δ_t	g_z
1	0.00	0.76×10^{-7}	38.567	0.00	0.62×10^{-7}	38.129
2	1.10	0.15×10^{-6}	6.750	1.31	0.12×10^{-6}	10.069



1

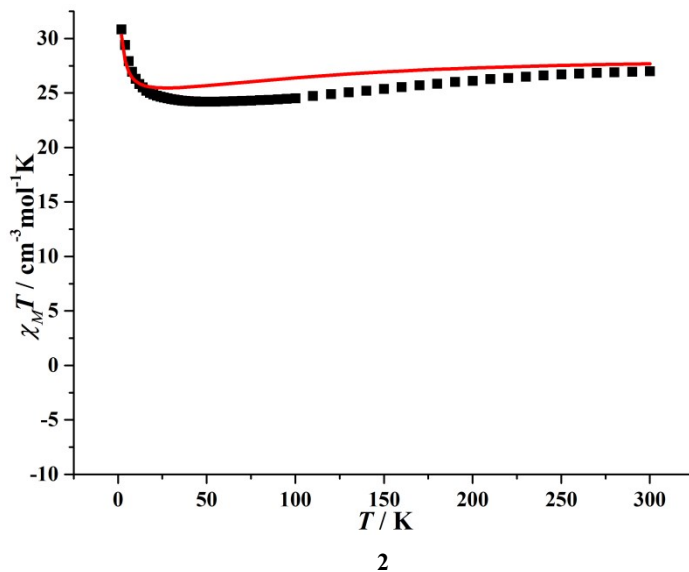


Fig. S12 Calculated (red solid line) and experimental (black square dot) data of magnetic susceptibilities of **1** and **2**. The intermolecular interactions zJ' of **1** and **2** were fitted to 0.01 and -0.01 cm^{-1} , respectively.

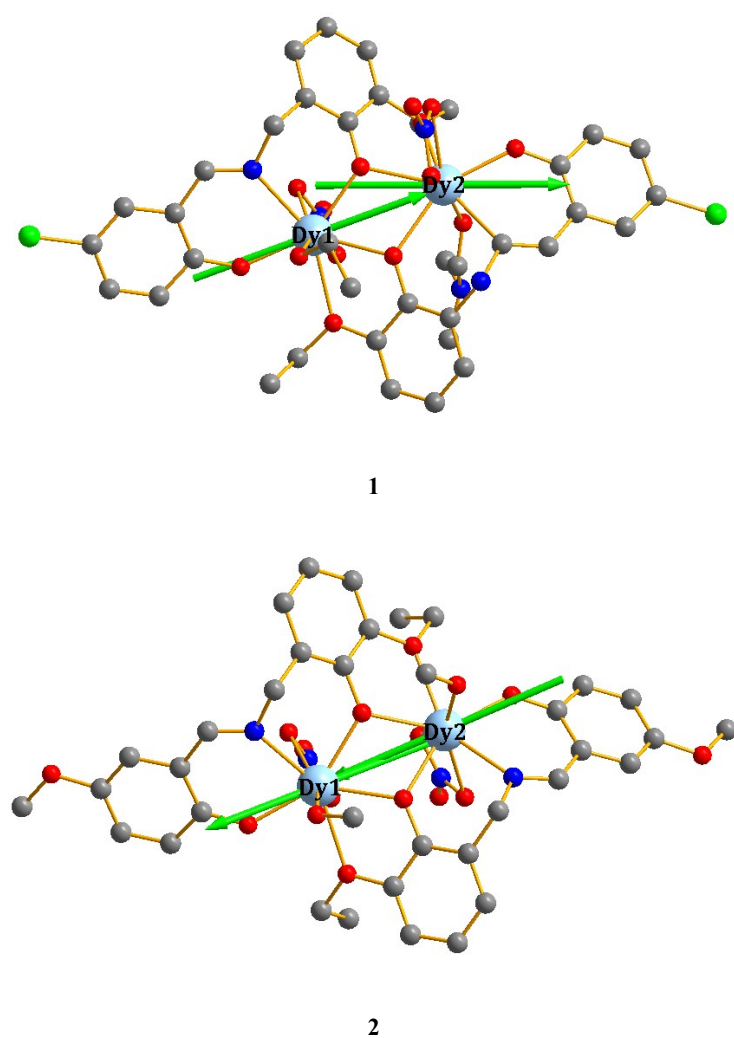


Fig. S13 Calculated orientations of the local main magnetic axes on Dy^{III} of complexes **1** and **2**.

References:

- S1 (a) X. F. Ma, B. B. Chen, Y. Q. Zhang, J. H. Yang, Q. Shi, Y. L. Ma and X. Y. Liu, *Dalton Trans.*, **2019**, *48*, 12622; (b) P. H. Lin, T. J. Burchell, R. Clerac and M. Murugesu, *Angew. Chem., Int. Ed.*, **2008**, *47*, 8848; (c) Y. Qin, H. F. Zhang, H. Sun, Y. D. Pan, Y. H. Ge, Y. H. Li and Y. Q. Zhang, *Chem. -Asian J.*, **2017**, *12*, 2834; (d) Y. R. Qin, Y. Jing, Y. Ge, W. Liu, Y. H. Li and Y. Q. Zhang, *Dalton Trans.*, **2018**, *48*, 15197; (e) K. Zhang, C. Yuan, F. S. Guo, Y. Q. Zhang and Y. Y. Wang, *Dalton Trans.*, **2016**, *46*, 186; (f) Y. Ge, Y. Huang, J. L. B. Montenegro, Y. F. Cui, W. Liu, Y. H. Li and B. L. Wang, *Chem. -Asian J.*, **2018**, *14*, 986.
- S2 F. Aquilante, J. Autschbach, R. K. Carlson, L. F. Chibotaru, M. G. Delcey, L. De Vico, I. Fdez. Galván, N. Ferré, L. M. Frutos, L. Gagliardi, M. Garavelli, A. Giussani, C. E. Hoyer, G. Li Manni, H. Lischka, D. Ma, P. Å. Malmqvist, T. Müller, A. Nenov, M. Olivucci, T. B. Pedersen, D. Peng, F. Plasser, B. Pritchard, M. Reiher, I. Rivalta, I. Schapiro, J. Segarra-Martí, M. Stenrup, D. G. Truhlar, L. Ungur, A. Valentini, S. Vancoillie, V. Veryazov, V. P. Vysotskiy, O. Weingart, F. Zapata, R. Lindh, MOLCAS 8: New Capabilities for Multiconfigurational Quantum Chemical Calculations across the Periodic Table, *J. Comput. Chem.* **2016**, *37*, 506.
- S3 (a) L. F. Chibotaru, L. Ungur, A. Soncini, *Angew. Chem., Int. Ed.*, **2008**, *47*, 4126. (b) L. Ungur, W. Van den Heuvel, L. F. Chibotaru, *New J. Chem.* **2009**, *33*, 1224. (c) L. F. Chibotaru, L. Ungur, C. Aronica, H. Elmoll, G. Pilet, D. Luneau, *J. Am. Chem. Soc.* **2008**, *130*, 12445-12455.
- S4 Lines, M. E. *J. Chem. Phys.* **1971**, *55*, 2977-2984.
- S5 (a) K. C. Mondal, A. Sundt, Y. H. Lan, G. E. Kostakis, O. Waldmann, L. Ungur, L. F. Chibotaru, C. E. Anson, A. K. Powell, *Angew. Chem., Int. Ed.* **2012**, *51*, 7550. (b) S. K. Langley, D. P. Wielechowski, V. Vieru, N. F. Chilton, B. Moubaraki, B. F. Abrahams, L. F. Chibotaru, K. S. Murray, *Angew. Chem., Int. Ed.* **2013**, *52*, 12014-12019.